# Partition of the electronic energy of the PM7 method via the Interacting Quantum Atoms approach

Hugo Salazar-Lozas[a], José Manuel Guevara-Vela[b], Angel Martín Pendás [c], Evelio Francisco[c] and Tomás Rocha-Rinza[*a]

## Abstract

Partitions of the electronic energy such as that provided by the Interacting Quantum Atoms (IQA) approach, have given valuable insights for numerous chemical systems and processes. Unfortunately, this kind of analyses may involve the integration of scalar fields over very irregular volumes, a condition which leads to a large and often prohibitive computational effort. These circumstances have limited the use of these energy partitions to systems comprised by a few tens of atoms at most. On the other hand, semiempirical methods have proved useful in the study of systems of several thousands of atoms. Therefore, the goal of this work is to carry out partitions of the semiempirical method PM7 in compliance with the IQA approach. For this purpose, we computed one- and two-atomic energetic contributions whose sum equals the PM7 electronic energy. We illustrate how one might exploit the partition of electronic energies computed via the PM7 method by considering small organic and inorganic molecules and the energetics of individual hydrogen bond interactions within several water clusters which include $(H_2O)_{30}$, $(H_2O)_{50}$ and $(H_2O)_{100}$. We also considered the solvation of the amphiphilic caprylate anion to exemplify how to exploit the energy partition proposed in this paper. Overall, this investigation shows how the approach put forward herein might give further insights of the interactions occurring within complex systems in physical and biological chemistry.

[a] *Instituto de Química, Universidad Nacional Autónoma de México, Circuito Exterior, Ciudad Universitaria, Alcaldía Coyoacán C.P. 04510, Ciudad de México, México. E-mail: trocha@iquimica.unam.mx*

[b] *MDEA Materials Institute, C/Eric Kandel 2, 28906 - Getafe, Madrid, Spain.*

[c] *Departamento de Química Física y Analítica, Universidad de Oviedo, Julián Claveria 8, 33006, Oviedo, España.*

# Introduction

The use of rapid methods of quantum chemistry is essential to investigate the electronic structure of systems comprised of hundreds or even thousands of atoms. There are nowadays very accurate methodologies to address medium-sized electronic systems ($\sim 10^2$ atoms) such as those based on ab initio wave function methods such as coupled cluster theory. One can also find reported DFT calculations which address systems with several thousands of atoms. Nevertheless, the computational investigation of large molecular clusters relies often on the exploitation of molecular dynamics simulations and Semi-empirical Methods (SM). SM[1] entail a simple strategy: they start from the formalism of Hartree-Fock (HF) theory and introduce assumptions to increase the speed of the underlying calculations. These considerations generally involve the omission of certain terms from the equations that define the HF method. In order to compensate for the errors inherent to these approximations, SM incorporate empirical parameters which are fit to experimental or highly accurate theoretical data.

The most widely used SM are variants of the Modified Neglect of Diatomic Overlap (MNDO)[2] model, which is based on the Neglect of Differential Diatomic Overlap (NDDO)[3] approximation for two-electron integrals. These MNDO-type methods include the AM1[4], PM3[5], PM6[6] and PM7[7] approximations among others. A common characteristic of these approaches is that they all pursue to improve the precision of the resulting electronic structure calculations via an extensive parameterisation which might include modifications of the nuclear repulsion functions. SM have been used in a large number of systems and processes to obtain molecular properties such as energetic gaps in fullerenes[8], prediction of protein structures[9] and modelling of catalytic mechanisms of enzymes[10], among other applications[11–13].

On the other hand, the computation of local properties such as atomic charges and interatomic interaction energies in molecules and molecular clusters has always been a challenge in physical chemistry. Some of the most popular electronic energy partitioning schemes used in chemistry include: (i) the Energy Decomposition Analysis (EDA)[14] which has as a variant (ii) the Natural Energy Decomposition Analysis (NEDA)[15], (iii) the Natural Bonding Orbitals (NBO) Analysis[16] and (iv) Quantum Chemical Topology (QCT)[17]. The domain of QCT includes the Quantum Theory of Atoms in Molecules[18] and the Interacting Quantum Atoms (IQA) energy partition[19]. The last-mentioned methodology has several attractive features such as its theoretical soundness, its quantification of the energetics of chemical interactions regardless of their nature and its rationalisation of the transferability of atoms,

functional groups and the interactions among them.[20–23] Furthermore, this energy partition has found many successful applications in physical chemistry[24–30]. The IQA approach has been exploited to gain valuable insights about different topics such as halogen and hydrogen bonds, steric repulsions, bond energies, chemical potentials and the nature of functional groups.[31–39] Notwithstanding, the computational cost of the IQA analyses is considerably high even for relatively small systems ($\sim$100 atoms)[40,41].

Due to the advantages that SM offer for the quantum chemical investigation of large electronic systems and the chemical insight provided by the IQA energy partition, we are interested in the coupling of SM with the IQA method of wave function analysis. This possibility would provide a tool to increase our understanding of intricate energetic interplays which take place in complex systems. Overall, our investigation shows how the IQA theoretical framework can be exploited to further understand different features of large systems suitably described by SM, in particular the quantification of the energetics of the chemical interactions occurring within them which ultimately govern their behaviour.

## Theoretical Background

The electronic energy in the IQA approach is divided in intra- ($E_{\text{net}}^{\text{A}}$), and inter-atomic ($E_{\text{int}}^{\text{AB}}$) contributions:

$$E = \sum_{\text{A}} E_{\text{net}}^{\text{A}} + \frac{1}{2} \sum_{\text{A} \neq \text{B}} E_{\text{int}}^{\text{AB}}, \tag{1}$$

in which

$$E_{\text{net}}^{\text{A}} = T^{\text{A}} + V_{\text{ne}}^{\text{AA}} + V_{\text{ee}}^{\text{AA}}, \tag{2}$$

$$E_{\text{int}}^{\text{AB}} = V_{\text{nn}}^{\text{AB}} + V_{\text{ne}}^{\text{AB}} + V_{\text{ne}}^{\text{BA}} + V_{\text{ee}}^{\text{AB}}. \tag{3}$$

The components to the intra- and inter-atomic energies are as follows. $T^{\text{A}}$ denotes the kinetic energy within atomic basin A while $V_{\text{ne}}^{\text{AA}}$ is the core-electron attraction and $V_{\text{ee}}^{\text{AA}}$ is the electronic repulsion inside the same basin A. On the other hand, $V_{\text{nn}}^{\text{AB}}$ is the repulsion between the cores A and B, $V_{\text{ne}}^{\text{AB}}$ is the interaction between core A and the electrons of atom B, and $V_{\text{ee}}^{\text{AB}}$ represents the repulsions between electrons in atoms A and B. Due to the partition of the pair density into Coulombic and exchange-correlation contributions,

$$\rho_2(\mathbf{r}_1, \mathbf{r}_2) = \rho(\mathbf{r}_1)\rho(\mathbf{r}_2) - \rho_2^{\text{xc}}(\mathbf{r}_1, \mathbf{r}_2)$$

$$= \rho_2^{\text{J}}(\mathbf{r}_1, \mathbf{r}_2) - \rho_2^{\text{xc}}(\mathbf{r}_1, \mathbf{r}_2), \tag{4}$$

both the intra- and inter-atomic electron-electron components can be split into Coulombic and exchange-correlation contributions

$$V_{\text{ee}}^{\text{AB}} = V_{\text{J}}^{\text{AB}} + V_{\text{xc}}^{\text{AB}}, \tag{5}$$

regardless whether A equals B or not.

The electronic energy partition according to the IQA approach (equation (1)) can be rewritten to compute the net and interaction energies among different molecules or more generally groups of atoms $\mathcal{G}$, $\mathcal{H}$, $\mathcal{I}$, ... Thus, the energy of the collection of atoms $\mathcal{G}$ reads,

$$E_{\text{net}}^{\mathcal{G}} = \sum_{A \in \mathcal{G}} E_{\text{net}}^{\text{A}} + \frac{1}{2} \sum_{A \in \mathcal{G}} \sum_{\substack{B \in \mathcal{G} \\ A \neq B}} E_{\text{int}}^{\text{AB}}. \tag{6}$$

On the other hand, the interaction energy between the groups of atoms $\mathcal{G}$ and $\mathcal{H}$ is given by,

$$E_{\text{int}}^{\mathcal{G}\mathcal{H}} = \sum_{A \in \mathcal{G}} \sum_{B \in \mathcal{H}} E_{\text{int}}^{\text{AB}}, \tag{7}$$

so that the electronic energy can be written as,

$$E = \sum_{\mathcal{G}} E_{\text{net}}^{\mathcal{G}} + \frac{1}{2} \sum_{\mathcal{G} \neq \mathcal{H}} E_{\text{int}}^{\mathcal{G}\mathcal{H}}. \tag{8}$$

The partition of the electronic energy of SM exploited herein rely on ideas developed firstly by Pople[3] and afterwards by Fischer and Kollmar[42]. These workers realized how the total molecular energy $E$ can be partitioned from the CNDO theory according to Equation 1 in intra- and inter-atomic terms respectively.

Hereof, the total molecular energy for a closed shell system is:

$$E = 2 \sum_{i} H_{ii} + 2 \sum_{ij} J_{ij} - \sum_{ij} K_{ij} + \sum_{A<B} \frac{Z_{\text{A}} Z_{\text{B}}}{R_{\text{AB}}}, \tag{9}$$

where the summations run over occupied $i, j \ldots$ SCF molecular orbitals. $H_{ii}$ is a diagonal matrix element of the monoelectronic Hamiltonian in the molecular orbital basis set. Likewise, the matrix elements $J_{ij}$ and $K_{ij}$ denote the interelectronic repulsion. Finally the last term in the RHS of equation (9) indicates the repulsion among nuclei. All these terms are

virtually equivalent to those in Hartree-Fock molecular orbital theory with the difference that the matrix elements for atomic basis functions $|\mu\rangle$ and $|\nu\rangle$ centred on different nuclei reads,

$$H_{\mu\nu} = \beta_{\mu\nu} S_{\mu\nu}, \qquad |\mu\rangle \in A \text{ and } |\nu\rangle \in B, \tag{10}$$

wherein $S_{\mu\nu}$ is the overlap of the atomic basis functions $\mu$ and $\nu$; and the index $\beta_{\mu\nu}$ is a parameter which depends on the types of orbitals $\mu$ and $\nu$[42].

Although the consideration of equation (10), does not alter expression (2), the monoelectronic part of the RHS of formula (3), $E_{\text{mono}}^{\text{AB}}$, has to be slightly modified,

$$E_{\text{mono}}^{\text{AB}} = V_{\text{ne}}^{\text{AB}} + V_{\text{ne}}^{\text{BA}} + E_{\text{R}}^{\text{AB}}, \tag{11}$$

in which,

$$E_{\text{R}}^{\text{AB}} = 2 \sum_{\mu \in A} \sum_{\nu \in B} P_{\mu\nu} \beta_{\mu\nu} S_{\mu\nu} \tag{12}$$

wherein $P_{\nu\mu}$ are the elements of the density matrix in the atomic basis set $\{\mu\}$. The resonance energy is a relevant feature of the energetics of the covalency of the interaction between A and B in semiempirical methods[42].

In summary, the partition of the electronic energy yielded by SM utilised herein has the following contributions:

1. Monoatomic energy components ($E_{\text{net}}^{\text{A}}$):

   - The monoelectronic energy in atom A is given by,

   $$T^{\text{A}} + V_{\text{ne}}^{\text{AA}} = \sum_{\mu \in A} P_{\mu\mu} U_{\mu\mu} = \sum_{\mu \in A} P_{\mu\mu} \left\langle \mu \left| -\frac{1}{2}\nabla^2 - \frac{Z_{\text{A}}}{r_{1\text{A}}} \right| \mu \right\rangle. \tag{13}$$

   This contribution equals the sum of the kinetic and the nucleus–electron potential energy within atom A. As implied above, $P_{\mu\mu}$ is a diagonal element of the density matrix in the atomic basis set. Ditto for $U_{\mu\mu}$ and the monoelectronic Hamiltonian. The index $Z_{\text{A}}$ is the core charge of atom A.

   - Classical interelectronic repulsion within atom A,

   $$V_{\text{J}}^{\text{AA}} = \frac{1}{2} \sum_{\mu \in A} \sum_{\nu \in A} P_{\mu\mu} P_{\nu\nu} \gamma_{\mu\nu}^{\text{AA}}, \tag{14}$$

   wherein $\gamma_{\mu\nu}^{\text{AA}} = \langle \mu\nu | \mu\nu \rangle$, is the Coulomb repulsion integral of two electrons in atom A with the basis functions $|\mu\rangle$ and $|\nu\rangle$ centred in A.

- Term of electronic exchange interaction in atom A,

$$V_{\text{xc}}^{\text{AA}} = -\frac{1}{4} \sum_{\mu \in A} \sum_{\nu \in A} P_{\mu\nu}^2 \gamma_{\mu\nu}^{\text{AA}}. \tag{15}$$

2. Interatomic energy components ($E_{\text{int}}^{\text{AB}}$):

- The monoelectronic energy between two atoms considered in Equation (11) is given by

$$V_{\text{ne}}^{\text{BA}} + V_{\text{ne}}^{\text{AB}} + V_{\text{R}}^{\text{AB}} = \sum_{\mu \in A} P_{\mu\mu} \left\langle \mu \left| -\frac{Z_B}{r_{1B}} \right| \mu \right\rangle + \sum_{\nu \in B} P_{\nu\nu} \left\langle \nu \left| -\frac{Z_A}{r_{1A}} \right| \nu \right\rangle$$
$$+ 2 \sum_{\mu \in A} \sum_{\nu \in B} P_{\mu\nu} \beta_{\mu\nu} S_{\mu\nu}, \tag{16}$$

where $V_{\text{R}}^{\text{AB}}$ is the component of the resonance energy for the bond A–B, and the basis functions $|\mu\rangle$ and $|\nu\rangle$ are centred on atoms A and B respectively.

- The quantity

$$V_{\text{J}}^{\text{AB}} = \sum_{\mu \in A} \sum_{\nu \in B} P_{\mu\mu} P_{\nu\nu} \gamma_{\mu\nu}^{\text{AB}}, \tag{17}$$

is the electronic Coulombic repulsion between atoms A and B, $\gamma_{\mu\nu}^{\text{AB}} = \langle \mu\nu | \mu\nu \rangle$ is the electronic repulsion integral between valence electrons, with $|\mu\rangle$ and $|\nu\rangle$ centred on atoms A and B respectively.

- Term of electronic exchange interaction among two atoms A and B,

$$V_{\text{xc}}^{\text{AB}} = -\frac{1}{2} \sum_{\mu \in A} \sum_{\nu \in B} P_{\mu\nu}^2 \gamma_{\mu\nu}^{\text{AB}}. \tag{18}$$

- Nuclear repulsion energy, which is given by,

$$V_{\text{nn}}^{\text{AB}} = Z_A Z_B \langle s_A s_A | s_B s_B \rangle \left( 1 + x_{AB} e^{-\alpha_{AB} R_{AB}} \right), \tag{19}$$

i.e., the repulsion energy between the cores of atoms A and B as Voityuk as Rösch represent[43]. $Z_A$ and $Z_B$ are the core charges atoms A and B, respectively. $\langle s_A s_A | s_B s_B \rangle$ is the two-center two-electron repulsion integral involving $s$ orbitals, $R_{AB}$ is the interatomic distance and $x_{AB}$ and $\alpha_{AB}$ are parameters for each pair of atoms A and B.

Finally, we point out that the above formalism is valid for the partition energy of a variety of SM as shown below.

## Computational details

We illustrate first the partition of the electronic energy computed with SM by considering small molecules ($H_2$, $N_2$, CO, $H_2O$, HClO and $NH_3$), the linear alkanes $C_nH_{2n+2}$ in which n = 1–6 and $C_{60}$ as well as the small water clusters $(H_2O)_n$ with n = 2–6 (Figure 1) and different structures of the water hexamer. Secondly, we examine the larger water clusters $(H_2O)_{30}$, $(H_2O)_{50}$ and $(H_2O)_{100}$ because of the utility of SM to deal with large systems. Finally, we consider the aqueous solvation of the amphiphilic caprylate anion. The geometry optimisations together with the computation of the corresponding wave functions of the molecular systems and the clusters $(H_2O)_n$ with n = 2–6, were performed with the semiempirical method PM7 as implemented in the package Mopac2016[44]. Concerning the clusters $(H_2O)_{30}$, $(H_2O)_{50}$ and $(H_2O)_{100}$ , as well as the solvation of the caprylate anion, we carried out Molecular Dynamics (MD) simulations in order to examine different configurations of the system. We used density functional tight binding with the third-order parameterisation for organic and biological systems[45] including the Tkatchenko and Scheffler estimation of van der Waals interactions[46] as implemented in the DFTB+ program[47] for every MD simulation considered herein. These calculations ran for 1000 steps with a step size of 1 fs using a Nose-Hoover thermostat set at 293 K. For the hydration of the caprylate anion, we set a cube with edges of 15 Å containing the anion and 200 water molecules. We let the geometry relax until the magnitude of the forces between atoms became smaller than $10^{-4}$ a.u. We used the resulting geometry as a initial point for the MD simulations for the hydration of the caprylate anion. Finally, we used the PM7 method to compute the corresponding energies by dint of the software Mopac2016 for geometries of interest.
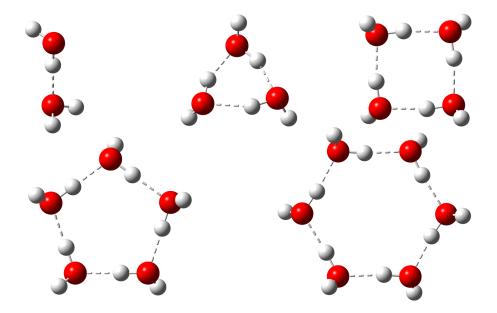
Figure 1: Small water clusters used to assess cooperative effects of hydrogen-bonding and the partition energy of the semiempirical method PM7.

## Results and discussion

We consider first the total sum of the intra- and inter-atomic terms of the partition of the electronic energy for the small molecules $H_2$, $N_2$, CO, $H_2O$, HClO, $NH_3$, $C_nH_{2n+2}$ (with n = 1–6), $C_{60}$ and the water clusters addressed herein. Table 1 shows that the sum of the net and interatomic components reproduce suitably the electronic energy of the examined systems. The maximum and average errors are $6.9 \times 10^{-2}$ and $3.5 \times 10^{-3}$ mHa respectively. These small errors give us confidence about the correctness of the implementation of the partition of the electronic energy of SM put forward in this paper. Table 2 shows the intra- and inter-atomic contributions of the electronic energy of the PM7 method for the systems considered in Table 1. Tables S1–S2 report the IQA partition for other SM such as MNDO, MNDO-D, AM1, PM3, PM6, PM6-D3, PM6-DH+, PM6-DH2, PM6-DH2X, PM6-D3H4, PM6-D3H4X and RM1 for the small molecules $H_2$, $N_2$, CO, $NH_3$ and HClO. In the rest of the paper, we will focus exclusively on the partition of PM7 interaction energies, which can give valuable physical insights about different interactions in complex systems. This circumstance is illustrated below in the addressed water clusters and the solvation of the amphiphilic caprylate anion.

## Partition of the PM7 electronic energy in small water clusters

We carried out the partition of the electronic energy yielded by the PM7 method and examined different features of hydrogen bonding as it is done in reference [48] which considered several different electronic structure methods such as HF, MP2, CCSD and several exchange-correlation functionals. First, we discuss H-bond cooperative effects in the formation of cyclic water clusters $(H_2O)_n$ n = 2–6. For that purpose, we consider the difference,

$$\Delta\Delta E_n = \Delta E_n - \Delta E_2, \tag{20}$$

in which $\Delta E_n$ is the change of energy of the system involved in the process

$$(H_2O)_{n-1} + H_2O \rightleftharpoons (H_2O)_n \text{ (with n = 2–6).} \tag{21}$$

A negative value of $\Delta\Delta E_n$ indicates that the addition of the n–th water molecule to $(H_2O)_{n-1}$ to form the cluster $(H_2O)_n$ is energetically more favourable than the generation of the single hydrogen bond within $(H_2O)_2$. The plot of $\Delta\Delta E_n$ as a function of n for different electronic structure methods is shown in Figure 2. This figure also illustrates that the PM7 behaviour of $\Delta\Delta E_n$ as n increases, i.e., throughout the sequential formation of water clusters, is similar to those already reported for different exchange-correlation functionals and wave function methods considered in references [48] and [49]. Furthermore, we observe a maximum and a minimum of $\Delta\Delta E_n$ for $(H_2O)_2$ and $(H_2O)_4$ respectively, in all the addressed methods of electronic structure considered in Figure 2 including PM7. The good description of non-additive effects of hydrogen bonding using the last-mentioned method will be further exploited to study the larger water clusters $(H_2O)_{30}$, $(H_2O)_{50}$ and $(H_2O)_{100}$ and the aqueous solvation of the caprylate anion.

Table 1: Values of IQA net, $\sum\limits_{\text{A}} E_{\text{net}}^{\text{A}}$, interaction, $\sum\limits_{\text{A}<\text{B}} E_{\text{int}}^{\text{AB}}$, and total, $\sum\limits_{\text{A}} E_{\text{net}}^{\text{A}} + \sum\limits_{\text{A}<\text{B}} E_{\text{int}}^{\text{AB}}$, electronic energies of the molecules and molecular clusters considered herein. The chart also displays the values of the molecular energies $E(\text{PM7})$ computed with Mopac2016. All values are reported in atomic units.

| | Partition of the PM7 electronic energy | | | |
|---|---|---|---|---|
| System | $\sum\limits_{\text{A}} E_{\text{net}}^{\text{A}}$ | $\sum\limits_{\text{A}<\text{B}} E_{\text{int}}^{\text{AB}}$ | $\sum\limits_{\text{A}} E_{\text{net}}^{\text{A}} + \sum\limits_{\text{A}<\text{B}} E_{\text{int}}^{\text{AB}}$ | $E(\text{PM7})$ |
| $H_2$ | −0.553643 | −0.477064 | −1.030707 | −1.030707 |
| $N_2$ | −12.362719 | −1.298088 | −13.660807 | −13.660807 |
| CO | −14.306646 | −1.032851 | −15.339498 | −15.339498 |
| HClO | −20.296703 | −0.809985 | −21.106689 | −21.106689 |
| $NH_3$ | −6.843848 | −1.489168 | −8.333016 | −8.333016 |
| $CH_4$ | −4.708801 | −1.797418 | −6.506219 | −6.506219 |
| $C_2H_6$ | −8.916656 | −3.099126 | −12.015783 | −12.015783 |
| $C_3H_8$ | −13.110386 | −4.416533 | −17.526919 | −17.526919 |
| $C_4H_{10}$ | −17.306186 | −5.732017 | −23.038204 | −23.038203 |
| $C_5H_{12}$ | −21.502493 | −7.046837 | −28.549330 | −28.549330 |
| $C_6H_{14}$ | −25.698685 | −8.361733 | −34.060418 | −34.060418 |
| $C_{60}$ | −219.019950 | −50.996964 | −270.016914 | −270.016912 |
| $H_2O$ | −10.899740 | −0.958503 | −11.858243 | −11.858243 |
| $(H_2O)_2$ | −21.788798 | −1.930412 | −23.719210 | −23.719210 |
| $(H_2O)_3$ | −32.671935 | −2.914201 | −35.586136 | −35.586136 |
| $(H_2O)_4$ | −43.554457 | −3.898346 | −47.452802 | −47.452803 |
| $(H_2O)_5$ | −54.435036 | −4.882160 | −59.317196 | −59.317196 |
| $(H_2O)_6(\text{ring})$ | −65.320046 | −5.862899 | −71.182945 | −71.182946 |
| $(H_2O)_6(\text{bag})$ | −65.325607 | −5.854867 | −71.180475 | −71.180474 |
| $(H_2O)_6(\text{book})$ | −65.322057 | −5.859326 | −71.181384 | −71.181384 |
| $(H_2O)_6(\text{cage})$ | −65.321617 | −5.857867 | −71.179484 | −71.179484 |
| $(H_2O)_6(\text{prism})$ | −65.322639 | −5.861055 | −71.183694 | −71.183694 |
| $(H_2O)_{30}$ | −326.792138 | −29.069024 | −355.861162 | −355.861163 |
| $(H_2O)_{50}$ | −544.641464 | −48.443449 | −593.084913 | −593.084919 |
| $(H_2O)_{100}$ | −1089.266148 | −96.886464 | −1186.152611 | −1186.152626 |
| $C_8H_{15}O_2^-$ $+H_2O_{200}$ | −2232.663668 | −204.352315 | −2437.015983 | −2437.016052 |

Table 2: Components of the partition of the PM7 electronic energy. All values are reported in atomic units.

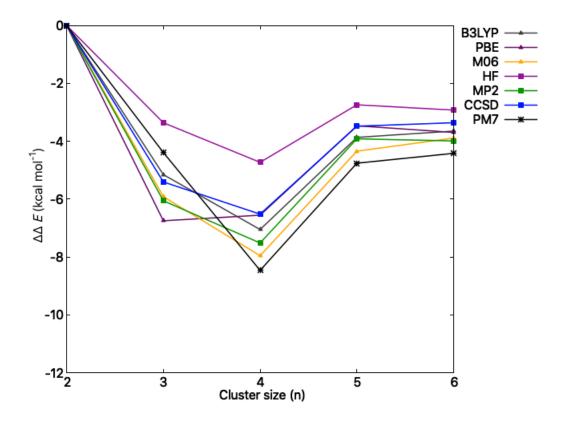| | | Partition of the PM7 electronic energy | | | |
|---|---|---|---|---|---|
| System | $T^{\mathrm{A}} + V_{\mathrm{ne}}^{\mathrm{AA}}$ | $V_{\mathrm{ee}}^{\mathrm{AA}}$ | $V_{\mathrm{R}}^{\mathrm{AB}}$ | $V_{\mathrm{xc}}^{\mathrm{AB}}$ | $V_{\mathrm{Cl}}^{\mathrm{AB}}$ |
| $H_2$ | $-0.813638$ | $0.259995$ | $-0.393976$ | $-0.208388$ | $0.125300$ |
| $N_2$ | $-19.701129$ | $7.338410$ | $-1.366801$ | $-0.559711$ | $0.628423$ |
| CO | $-24.492035$ | $10.185389$ | $-1.057182$ | $-0.425338$ | $0.449669$ |
| HClO | $-34.040849$ | $13.744146$ | $-0.841737$ | $-0.343650$ | $0.375402$ |
| $NH_3$ | $-11.977021$ | $5.133173$ | $-1.566223$ | $-0.601435$ | $0.678491$ |
| $CH_4$ | $-8.602671$ | $3.893870$ | $-1.734276$ | $-0.784556$ | $0.721414$ |
| $C_2H_6$ | $-15.999712$ | $7.083056$ | $-3.008191$ | $-1.360549$ | $1.269613$ |
| $C_3H_8$ | $-23.439748$ | $10.329362$ | $-4.288481$ | $-1.934818$ | $1.806767$ |
| $C_4H_{10}$ | $-30.886254$ | $13.580067$ | $-5.568416$ | $-2.508685$ | $2.345084$ |
| $C_5H_{12}$ | $-38.328624$ | $16.826131$ | $-6.848422$ | $-3.082848$ | $2.884433$ |
| $C_6H_{14}$ | $-45.769387$ | $20.070702$ | $-8.128494$ | $-3.657050$ | $3.423810$ |
| $C_{60}$ | $-380.573491$ | $161.553541$ | $-50.377675$ | $-21.458050$ | $20.838762$ |
| $H_2O$ | $-19.586379$ | $8.686639$ | $-0.967809$ | $-0.375629$ | $0.384935$ |
| $(H_2O)_2$ | $-39.301856$ | $17.513058$ | $-1.941702$ | $-0.741114$ | $0.752405$ |
| $(H_2O)_3$ | $-59.184396$ | $26.512461$ | $-2.888312$ | $-1.089704$ | $1.063815$ |
| $(H_2O)_4$ | $-79.009699$ | $35.455242$ | $-3.845640$ | $-1.444203$ | $1.391498$ |
| $(H_2O)_5$ | $-98.798313$ | $44.363277$ | $-4.813267$ | $-1.803264$ | $1.734371$ |
| $(H_2O)_6$(ring) | $-118.591376$ | $53.271330$ | $-5.771972$ | $-2.161513$ | $2.070585$ |
| $(H_2O)_6$(bag) | $-118.566124$ | $53.240517$ | $-5.768390$ | $-2.162111$ | $2.075634$ |
| $(H_2O)_6$(book) | $-118.589941$ | $53.267884$ | $-5.769872$ | $-2.160286$ | $2.070831$ |
| $(H_2O)_6$(cage) | $-118.635095$ | $53.313478$ | $-5.768260$ | $-2.154266$ | $2.064659$ |
| $(H_2O)_6$(prism) | $-118.698376$ | $53.375737$ | $-5.751626$ | $-2.147954$ | $2.038525$ |
| $(H_2O)_{30}$ | $-591.329206$ | $264.537068$ | $-28.592474$ | $-10.941929$ | $10.465379$ |
| $(H_2O)_{50}$ | $-986.276668$ | $441.635204$ | $-47.426054$ | $-18.156074$ | $17.138680$ |
| $(H_2O)_{100}$ | $-1972.653558$ | $883.387411$ | $-94.767897$ | $-36.289509$ | $34.170943$ |
| $C_8H_{15}O_2^-$ $+(H_2O)_{200}$ | $-4046.655376$ | $1813.991708$ | $-200.801459$ | $-76.375977$ | $72.825121$ |

Figure 2: Plot of $\Delta\Delta E_n$ (Equation (17)) as a function of n for different electronic structure methods. The cooperative effects of hydrogen bond in the formation of clusters $(H_2O)_n$ are evidenced through negative values of $\Delta\Delta E_n$. The data computed with ab initio methods and DFT exchange correlation functionals were taken from reference [48].

Non-additive effects of hydrogen bonding can also be examined via partitions of the electronic energy. For this purpose, we consider (i) the interaction energy between monomers $\mathcal{G}$ and $\mathcal{H}$ ($E_{\text{int}}^{\mathcal{GH}}$) in equation (7), (ii) the deformation energy of monomer $\mathcal{G}$ ($E_{\text{def}}^{\mathcal{G}}$) and (iii) the change of energy associated to the formation of a molecular cluster $\mathcal{G}\cdots\mathcal{H}\cdots$, $E_{\text{form}}^{\mathcal{G}\cdots\mathcal{H}\cdots}$. The value of $E_{\text{def}}^{\mathcal{G}}$ and $E_{\text{form}}^{\mathcal{G}\cdots\mathcal{H}\cdots}$ can be computed as,

$$E_{\text{def}}^{\mathcal{G}} = E_{\text{net}}^{\mathcal{G}} - E_{\text{iso}}^{\mathcal{G}}, \tag{22}$$

$$E_{\text{form}}^{\mathcal{G}\cdots\mathcal{H}\cdots} = \sum_{\mathcal{G}} E_{\text{def}}^{\mathcal{G}} + \sum_{\mathcal{G}} \sum_{\mathcal{G}>\mathcal{H}} E_{\text{int}}^{\mathcal{GH}}. \tag{23}$$

These equations indicate that (i) $E_{\text{def}}^{\mathcal{G}}$ is the difference of energy of $\mathcal{G}$ within the cluster $\mathcal{G}\cdots\mathcal{H}\cdots$ and its isolated equilibrium configuration, $E_{\text{iso}}^{\mathcal{G}}$, and (ii) $E_{\text{form}}^{\mathcal{G}\cdots\mathcal{H}\cdots}$ can be calculated in terms of $E_{\text{def}}^{\mathcal{G}}$ and $E_{\text{int}}^{\mathcal{GH}}$. Figure 3 shows the results for the formation, interaction and
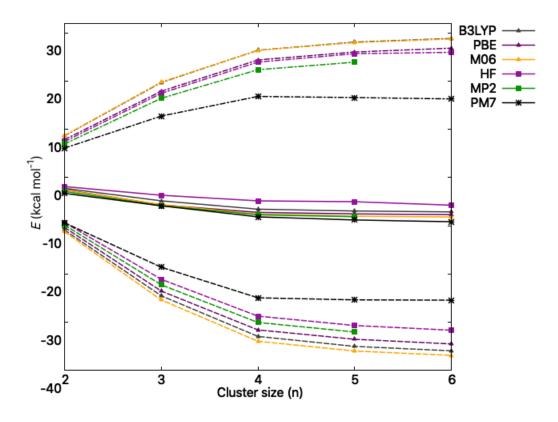
Figure 3: Deformation energies (dashed-dotted line), interaction energies (dashed line) and formation energies (solid line) per molecule as function of the water clusters shown in Figure 1. Several different methods of electronic structure theory are considered in the figure.

deformation energies for the water clusters $(H_2O)_n$ with n = 2 – 6. Likewise the previous analysis of $\Delta\Delta E_n$, the values for $E_{form}^{\mathcal{G}\cdots\mathcal{H}\cdots}$, $E_{int}^{\mathcal{G}\mathcal{H}}$ and $E_{def}^{\mathcal{G}}$ obtained from PM7 calculations are qualitatively similar to these computed with exchange-correlation calculations as well as with Hartree-Fock and correlated approximations to electronic wave functions[26,48,49].

**Partition of the PM7 electronic energy in different structures of the water hexamer.**

Non-additivy of hydrogen bonding can lead to both strengthening (cooperativity) or weakening (anticooperativity) of these interactions. Water clusters have become an archetype for the study of these two kinds of effects. The previously discussed water clusters comprise one single ring in which every single molecule acts as a single donor and a single acceptor (Figure 1). These motifs are associated with hydrogen bond cooperativity. Nevertheless, water molecules can act as double acceptors and donors, a circumstance which results in notorious cooperative and anticooperative effects as examined below. The water hexamer is the smallest $H_2O$ cluster whose potential energy hypersurface has local minima with monomers which are acceptors and donors with different coordination numbers. We consider here five different local minima of $(H_2O)_6$ shown in Figure 4. We also take into account a pairwise sum of interaction energies between monomers which equals the formation energy of the cluster, $E_{\text{form}}^{\mathcal{G}\cdots\mathcal{H}\cdots}$,

$$
\begin{aligned}
E_{\text{form}}^{\mathcal{G}\cdots\mathcal{H}\cdots} &= \sum_{\mathcal{G}} \sum_{\mathcal{G}>\mathcal{H}} \left( E_{\text{int}}^{\mathcal{G}\mathcal{H}} + \left( \frac{E_{\text{int}}^{\mathcal{G}\mathcal{H}}}{\displaystyle\sum_{\mathcal{J}\neq\mathcal{G}} E_{\text{int}}^{\mathcal{J}\mathcal{G}}} \right) E_{\text{def}}^{\mathcal{G}} + \left( \frac{E_{\text{int}}^{\mathcal{G}\mathcal{H}}}{\displaystyle\sum_{\mathcal{J}\neq\mathcal{H}} E_{\text{int}}^{\mathcal{J}\mathcal{H}}} \right) E_{\text{def}}^{\mathcal{H}} \right) \\
&= \sum_{\mathcal{G}} \sum_{\mathcal{G}>\mathcal{H}} E_{\text{int}}^{\mathcal{G}\mathcal{H}'}.
\end{aligned}
\tag{24}
$$

Figure 4 reports the values of $E_{\text{int}}^{\mathcal{G}\mathcal{H}'}$ for pairs of hydrogen-bonded monomers in the investigated configurations of $(H_2O)_6$. The partition of the PM7 electronic energy indicates that single Hydrogen Bond (HB) acceptors and donors are associated to HB cooperative effects while those HB monomers which involve double donors and acceptors are related to both cooperative and anticooperative effects of hydrogen bonding. These results are in agreement with those based on the division of correlated electronic energies[26]. We also considered the strengthening and weakening of HBs due to the formation of new hydrogen bond interactions. For example, Figure 5 shows the change in HB formation energy by virtue of the interaction of the water dimer and tetramer to generate the book and prism configurations of the water hexamer. Once again, we note that the PM7 prediction of the strengthening or weakening of hydrogen bonds due to the formation of larger clusters agree quantitatively with those yielded by the wave function analyses of correlated wave functions[26]. This observation indicates that the partition of the PM7 electronic energy can give valuable insights about H-bond non-additive effects in water clusters. Furthermore, they open up the possibility to
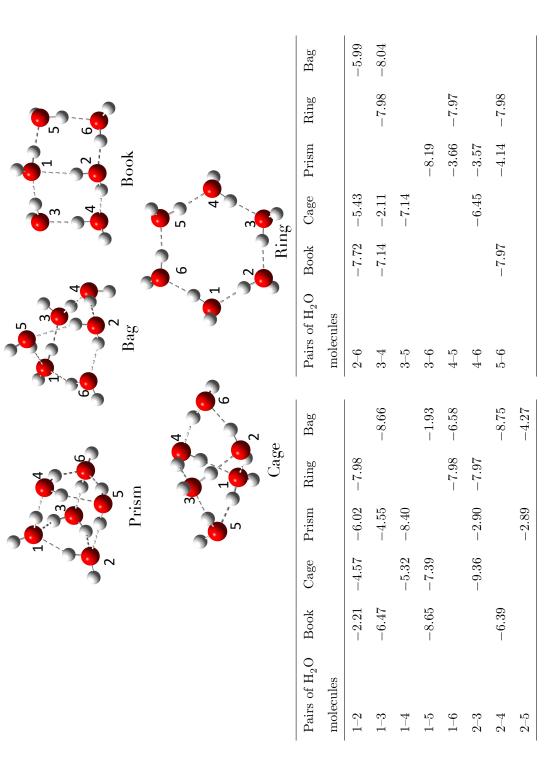
Figure 4: Top. Different structures of the water hexamer addressed herein. Bottom. Interaction energies (kcal/mol), $E_{int}^{\mathcal{GH}'}$ in equation (24), among pairs of hydrogen-bonded molecules within these configurations of $(H_2O)_6$.

| Pairs of H₂O molecules | Book | Cage | Prism | Ring | Bag |
|---|---|---|---|---|---|
| 1–2 | −2.21 | −4.57 | −6.02 | −7.98 | |
| 1–3 | −6.47 | | −4.55 | | −8.66 |
| 1–4 | −8.65 | −5.32 | −8.40 | | |
| 1–5 | | −7.39 | | | −1.93 |
| 1–6 | | | | −7.98 | −6.58 |
| 2–3 | | −9.36 | −2.90 | −7.97 | |
| 2–4 | −6.39 | | | | −8.75 |
| 2–5 | | | −2.89 | | −4.27 |

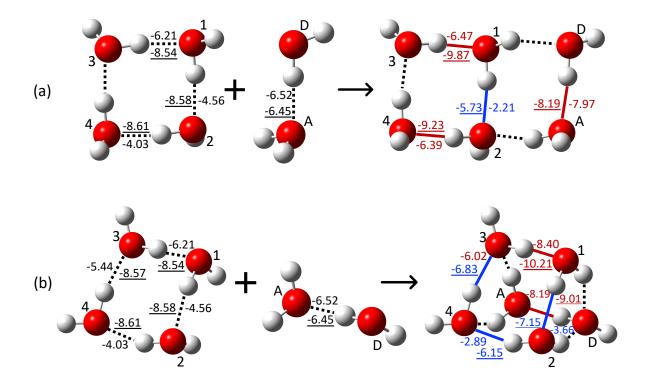| Pairs of H₂O molecules | Book | Cage | Prism | Ring | Bag |
|---|---|---|---|---|---|
| 2–6 | −7.72 | −5.43 | | | −5.99 |
| 3–4 | −7.14 | −2.11 | | −7.98 | −8.04 |
| 3–5 | | −7.14 | | | |
| 3–6 | | | −8.19 | | |
| 4–5 | | | −3.66 | −7.97 | |
| 4–6 | | −6.45 | −3.57 | | |
| 5–6 | −7.97 | | −4.14 | −7.98 | |

Figure 5: Formation of the book, (a), along with the prism (b) structure of $(H_2O)_6$ as a result of the interaction of smaller water clusters. The hydrogen bonds which are strengthened or weakened due to the formation of the corresponding hexamer are shown in red and blue respectively. The values of the interaction energies ($E_{\text{int}}^{H_2O\cdots H_2O'}$ according to equation (24)) are reported in kcal/mol. The underlined values of (a) and (b) were computed via the partition of MP2 electronic energies and are taken from reference [26].
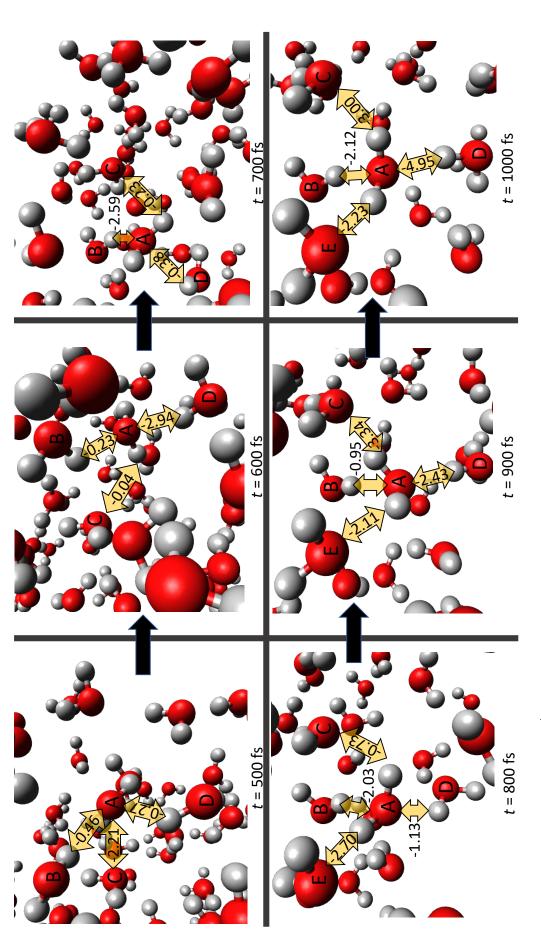
perform the partition of the PM7 electronic energy in phenomena that are suitably described by SM (e.g. hydrogen bond cooperativity and anticooperativity). We conclude this section by pointing out that there are other effects due to non-covalent interactions with similar interpretation yielded by the partition of the electronic energy of (i) semiempirical methods on one hand and (ii) ab initio approximations on the other. One example of this statement is the *trans* effect in the staggered conformation of ethane, in which *trans* hydrogens have a more attractive interaction energy than those with a dihedral angle $\phi = 60$ as a result of the different covalent contributions to the electronic energy in these pairs of atoms[42].

**Partition of the PM7 electronic energy in the water clusters $(H_2O)_n$ n = 30, 50, 100 and the aqueous solvation of the caprylate anion.**

We consider now the water clusters $(H_2O)_{30}$, $(H_2O)_{50}$ and $(H_2O)_{100}$, to further illustrate the capabilities of the PM7 electronic energy put forward herein. We consider molecular dynamics simulations of these systems for a total time of 1 ps in steps of 1 fs. Figure 6 shows the values of $E_{int}^{\mathcal{GH}'}$ for a specific water molecule inside the cluster $(H_2O)_{100}$. Tables S3-S9 in the ESI, report the interaction energies associated to hydrogen-bonded molecules within $(H_2O)_{50}$ and $(H_2O)_{100}$. The last-mentioned figure and tables exemplify how the approach presented herein can be exploited along SM calculations. We stress that the empirical HB energies yielded by SM are in many cases far smaller than those that could be expected from the potential energy surface of $(H_2O)_2$, e.g. around $-1.0$ kcal/mol in average for $(H_2O)_{30}$. The approach addressed here ameliorates this situation and presents a better assessment of the individual interactions between water molecules in the system via equation (24). We expect that these improvements would be also observed in the examination of other complex supramolecular systems examined via SM. We note that the interaction between water monomers, e.g., A–D in Figure 6, can be relatively small in magnitude or even repulsive. This circumstance occurs due to the relative orientation of the interacting monomers which is the result of the contacts with other $H_2O$ molecules in the system.

Now, we consider the caprylate anion $(C_8H_{15}O_2^-)$ solvated by 200 $H_2O$ molecules. We address first the interaction energies $E_{int}^{\mathcal{GH}'}$ between the $C_8H_{15}O_2^-$ anion and its first solvation shell around its hydrophilic –COO$^-$ group. Table 3 shows the values of $E_{IQA}^{\mathcal{GH}}$ and $E_{IQA}^{\mathcal{GH}'}$ in equations (7) and (24) respectively wherein $\mathcal{G} = C_8H_{15}O_2^-$ and $\mathcal{H}$ is a water molecule which is directly H-bonded to the carboxylate moiety. We note that $|E_{int}^{\mathcal{GH}'}| \ll |E_{int}^{\mathcal{GH}}|$ for the interactions between the caprylate anion and its first solvation shell forming hydrogen bonds with the –COO$^-$ group. This substantial difference is due to the very large deformation energy of the caprylate anion $E_{def}^{C_8H_{15}O_2^-} = 89$ kcal/mol. We conjectured that the hydrophobic tail of the caprylate anion contributes largely to $E_{def}^{C_8H_{15}O_2^-}$, a condition which reduces drastically the value of $E_{int}^{\mathcal{GH}'}$ in the assessment of the interaction between the negatively charged oxygens of the carboxylate group and the surrounding water molecules. Therefore, we further divide the caprylate anion in eight different fragments: the methyl, the methylene and the carboxylate groups:

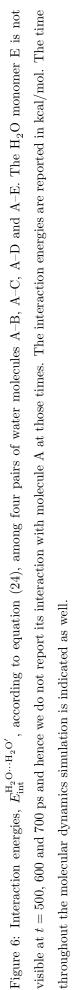$$CH_3 \diagup CH_2 \diagup CH_2 \diagup CH_2 \diagup CH_2 \diagup CH_2 \diagup CH_2 \diagup COO^-$$

Figure 6: Interaction energies, $E_{\text{int}}^{\text{H}_2\text{O}\cdots\text{H}_2\text{O}'}$, according to equation (24), among four pairs of water molecules A–B, A–C, A–D and A–E. The $\text{H}_2\text{O}$ monomer E is not visible at $t = 500$, 600 and 700 ps and hence we do not report its interaction with molecule A at those times. The interaction energies are reported in kcal/mol. The time throughout the molecular dynamics simulation is indicated as well.

18

Table 3: IQA interaction energies, $E_{\text{IQA}}^{\mathcal{GH}}$ and $E_{\text{IQA}}^{\mathcal{GH}\prime}$ in expressions (7) and (24) respectively, between the complete caprylate anion and the water molecules interacting directly with the carboxylate moiety. The values are reported in kcal/mol and the labels of the water molecules are also displayed.

| Pair | $E_{\text{IQA}}^{\mathcal{GH}}$ | $E_{\text{IQA}}^{\mathcal{GH}\prime}$ |
|---|---|---|
| $C_7H_{15}COO^- \cdots H_2O(92)$ | $-22.82$ | $-3.39$ |
| $C_7H_{15}COO^- \cdots H_2O(117)$ | $-12.91$ | $-2.05$ |
| $C_7H_{15}COO^- \cdots H_2O(180)$ | $-19.93$ | $-2.53$ |
| $C_7H_{15}COO^- \cdots H_2O(12)$ | $-16.75$ | $-1.40$ |
| $C_7H_{15}COO^- \cdots H_2O(89)$ | $-19.64$ | $-0.48$ |
| $C_7H_{15}COO^- \cdots H_2O(162)$ | $-10.48$ | $-1.99$ |

Indeed, this division of the caprylate anion reveals that more than 45% of the deformation energy of the $C_8H_{15}O_2^-$ ion ($\approx 41$ kcal/mol) is associated to the hydrocarbon chain of this amphiphilic species. Figure 7 reveals the values of $E_{\text{IQA}}^{\mathcal{GH}}$ between the –COO$^-$ group and the water molecules surrounding this moiety. We observe a fairly wide range of interactions energies ranging roughly from $-3.30$ to $-9.76$ kcal/mol. We note strongly anticooperative effects, i.e. the mutual weakening of H-bonds in a system, in the interactions between the carboxylate group and the water molecules surrounding it. We computed the formation energy between a caprylate anion and a water molecule ($C_8H_{15}O_2^- \cdots H_2O$) using the approximation MP2/aug-cc-pVTZ//PBE/aug-cc-pVTZ, i.e., $\Delta E_{\text{form}}^{C_8H_{15}O_2^- \cdots H_2O} = -18.89$ kcal/mol. All the hydrogen bonds –COO$^- \cdots H_2O$ shown in Figure 7 are of smaller magnitude than $\Delta E_{\text{form}}^{C_8H_{15}O_2^- \cdots H_2O}$. We put forward two reasons for such H-bond anticooperativity:

- the occurrence of other water molecules in the system substantially alters the optimal orientation of the $H_2O$ monomers for their interaction with –COO$^-$ and

- the electronic charge transfer from the carboxylate to the water molecules should be shared among all the hydrogen-bond donors interacting directly with the –COO$^-$ group as described in Figure 8. Indeed, the occurrence of multiple hydrogen bond acceptors has been identified as a source of H-bond anticooperativity[26,50–52]

Figure 7 shows the interactions of the first solvation shell with the hydrocarbon chain. As expected, the individual interactions of the water molecules with the –COO$^-$ moiety are larger in magnitude than those with the hydrocarbon chain (from 0.10 to 1.22 kcal/mol). Nevertheless, the partition of the PM7 electronic energy allows us to quantitatively evaluate such differences, i.e., allows to examine the interaction of distinct parts of the solute with the solvent.

Finally, we consider the interactions between the first and the second solvation shells
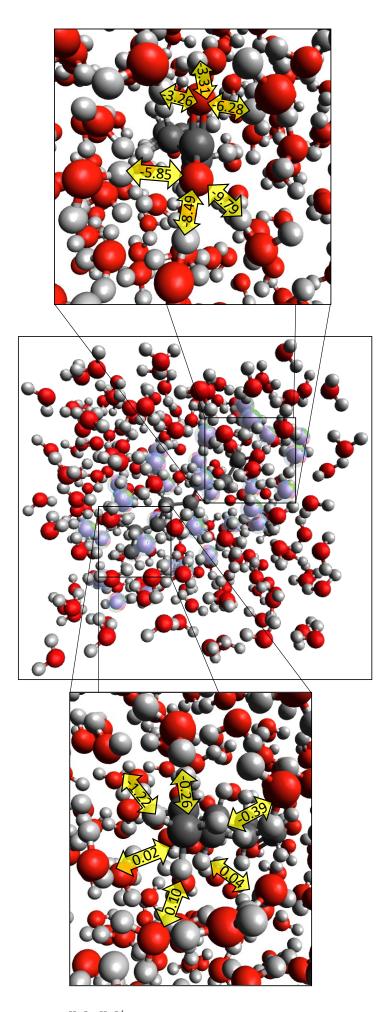
Figure 7: Interaction energies, $E_{\text{int}}^{\text{H}_2\text{O}\cdots\text{H}_2\text{O}'}$ according to equation (24), between the first solvation shell of the hydrophobic (left) and hydrophilic (right) of the caprylate anion in the aqueous solvation of this species. The interaction energies are reported in kcal/mol.
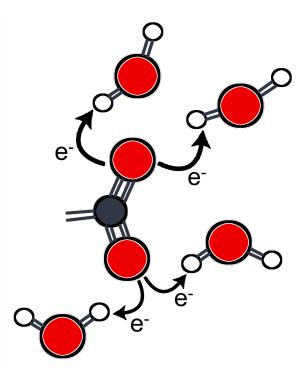
Figure 8: Schematisation of the electron charge donation from the carboxylate moiety of the caprylate anion to the hydrogen-bonding $H_2O$ molecules surrounding the $-COO^-$ functional group.

around the hydrophobic and the hydrophilic moieties around the caprylate anion in Table 4. The individual H-bonds between the first and the second solvation shell around the hydrophobic chain are weaker than they are around the $-COO^-$ hydrophilic group. This observation could naturally been anticipated in virtue of the polarising effects of the carboxylate on the first solvation shell. All these observation reveal the complexity of the interaction between a solute and its solvation shells. This type of analysis could provide valuables insights about the solvation of different sorts of systems such as biomolecules and we expect it would prove useful to examine complex phenomena in detail as the hydrophobic effect.

Table 4: IQA interaction energies, $E_{\text{IQA}}^{\mathcal{GH}\prime}$ in formula (24) between the first and second solvation shells for the caprylate anion around the hydrophilic and hydrophobic parts of this amphiphilic system. The values are reported in kcal/mol and the values of the water molecules are also displayed.

| Hydrophilic moiety | | Hydrophobic moiety | |
|---|---|---|---|
| Pair | $E_{\text{IQA}}^{\mathcal{GH}}$ | Pair | $E_{\text{IQA}}^{\mathcal{GH}}$ |
| $H_2O(92)\cdots H_2O(91)$ | $-0.66$ | $H_2O(18)\cdots H_2O(164)$ | $-0.42$ |
| $H_2O(117)\cdots H_2O(120)$ | $-2.72$ | $H_2O(19)\cdots H_2O(23)$ | $-0.23$ |
| $H_2O(180)\cdots H_2O(84)$ | $-1.82$ | $H_2O(20)\cdots H_2O(23)$ | $-0.10$ |
| $H_2O(12)\cdots H_2O(9)$ | $-1.04$ | $H_2O(22)\cdots H_2O(188)$ | $-2.31$ |
| $H_2O(89)\cdots H_2O(189)$ | $2.87$ | $H_2O(153)\cdots H_2O(133)$ | $-1.10$ |
| $H_2O(162)\cdots H_2O(75)$ | $-1.18$ | $H_2O(147)\cdots H_2O(40)$ | $0.46$ |

## Conclusions

We have presented herein a partition of the electronic energy of the PM7 method according to the formalism of the IQA method of wave function analysis. For this endeavour, we split these electronic energies $E$ in intra- and inter-atomic terms whose sums recover the total value of the electronic energy. We illustrated the partition of the electronic energy put forward herein in small organic and inorganic molecules as well as hydrogen-bonded clusters containing until 100 interacting monomers. We also considered the solvation of the amphiphilic caprylate anion by 200 $H_2O$ molecules. Concerning the smallest clusters, our partition described both cooperative and anticooperative H-bond effects in consistency with more sophisticated approximations of electronic wave functions and different exchange-correlation functionals. The consideration of the larger clusters show how different interactions among individual molecules can be computed throughout molecular dynamics simulations. This kind of analysis could be exploited in other situations of biological and chemical interest, such as conformational equilibria or drug-protein interactions. Altogether, we expect that the method of analysis presented herein will prove useful in the exploration of interactions wherein semiempirical methods might be useful, for example, in chemical and biological systems comprised of hundreds or even thousands of atoms.

## Acknowledgments

## References

[1] J. A. Pople and D. Beveridge, *Approximate Molecular Orbital Theory*, McGraw-Hill/Interamericana, 1970, pp. 57–83.

[2] M. J. S. Dewar and W. Thiel, *J. Am. Chem. Soc.*, 1977, **99**, 4899–4907.

[3] J. A. Pople, D. P. Santry and G. A.Segal, *J. Chem. Phys*, 1965, **43**, S129–S135.

[4] M. J. S. Dewar, E. G. Zoebisch, E. F. Healy and J. J. P. Stewart, *J. Am. Chem. Soc.*, 1985, **107**, 3902–3909.

[5] J. J. P. Stewart, *J. Comput. Chem.*, 1988, **10**, 209–220.

[6] J. J. P. Stewart, *J. Mol. Model.*, 2007, **13**, 1173–1213.

[7] J. J. P. Stewart, *J. Mol. Model.*, 2013, **19**, 1–32.

[8] C. Sikorska and T. Puzyn, *Nanotechnology*, 2015, **26**, 455702.

[9] B. P. Martin, C. J. Brandon, J. J. P. Stewart and S. B. Braun-Sand, *Proteins*, 2015, **83**, 1427–1435.

[10] J. J. P. Stewart, *J. Mol. Model.*, 2017, **23**, 154.

[11] H. M. Senn, J. Kastner, J. Breidung and W. Thiel, *Can. J. Chem.*, 2009, **87**, 1322–1337.

[12] M. A. Thompson and G. K. Schenter, *J. Phys. Chem.*, 1995, **99**, 6374–6386.

[13] I. Polyak, M. T. Reetz and W. Thiel, *J. Am. Chem. Soc.*, 2012, **87**, 1322–1337.

[14] M. V. Hopffgarten and G. Frenking, *Comput. Mol. Sci.*, 2012, **2**, 43–62.

[15] E. D. Glendening and A. Streitwieser, *Spectrochim. Acta Part A*, 1994, **100**, 2900–2909.

[16] D. Sajana, L. Josepha, N. Vijayanb and M. Karabacak, *Spectrochim. Acta Part A*, 2011, **81**, 85–98.

[17] C. F. Matta and J. B. Russell, *The Quantum Theory of Atoms in Molecules: From Solid State to DNA, Drug Design*, Wiley-VCH, 2007, pp. 1–16.

[18] R. Bader, *Atoms in Molecules: A Quantum Theory*, Oxford University Press, 1990.

[19] M. A. Blanco, A. Martín Pendás and E. Francisco, *J. Chem. Theory Comput.*, 2005, **1**, 1096–1109.

[20] I. Alkorta, I. Mata, E. Molins and E. Espinosa, *Chem. Eur. J.*, 2016, **22**, 9226–9234.

[21] O. J. Backhouse, J. C. R. Thacker and P. L. A. Popelier, *ChemPhysChem*, 2019, **20**, 555–564.

[22] M. Aarabi, S. Gholami and S. J. Grabowski, *ChemPhysChem*, 2020, **21**, 1653–1664.

[23] S. Li, A. Azizi, S. R. Kirk and S. Jenkins, *Int J Quantum Chem*, 2020, **120**,.

[24] O. A. Syzgantseva, V. Tognetti and L. Joubert, *J. Phys. Chem. A*, 2013, **117**, 8969–8980.

[25] A. Martín Pendás, M. A. Blanco and E. Francisco, *J. Chem. Phys*, 2006, **125**, 184112.

[26] J. M. Guevara-Vela, E. Romero-Montalvo, V. A. Mora-Gómez, R. Chávez-Calvillo, M. García-Revilla, E. Francisco, A. Martín Pendás and T. Rocha-Rinza, *Phys. Chem. Chem. Phys.*, 2016, **18**, 19485–19978.

[27] K. Eskandari and C. V. Alsenoy, *J. Comput. Chem.*, 2014, **35**, 1883–1889.

[28] E. Francisco, A. Martín Pendás and M. A. Blanco, *J. Chem. Theory Comput.*, 2005, **2**, 90–102.

[29] I. Alkorta, J. C. R. Thacker and P. L. A. Popelier, *J. Comput. Chem.*, 2018, **39**, 564–556.

[30] M. García-Revilla, E. Francisco, P. L. A. Popelier and A. Martín Pendás, *ChemPhysChem.*, 2013, **14**, 1211–1218.

[31] I. Alkorta, C. Martín-Fernández, M. M. Montero-Campillo and J. Elguero, *J. Phys. Chem. A*, 2018, **122**, 1472–1478.

[32] G. Sánchez-Sanz, C. Trujillo, I. Alkorta and J. Elguero, *ChemPhysChem*, 2020, **21**, 2557–2563.

[33] V. Tognetti and L. Joubert, *Theor. Chem. Acc.*, 2016, **135**,.

[34] M. Yahia-Ouahmed, V. Tognetti and L. Joubert, *Comput. Theor. Chem.*, 2015, **1053**, 254–262.

[35] J. R. Lane, J. Contreras-García, J.-P. Piquemal, B. J. Miller and H. G. Kjaergaard, *J. Chem. Theory Comput.*, 2013, **9**, 3263–3266.

[36] C. F. Matta, A. A. Arabi and T. A. Keith, *J. Phys. Chem. A*, 2007, **111**, 8864–8872.

[37] I. Mata, E. Molins, I. Alkorta and E. Espinosa, *J. Phys. Chem. A*, 2014, **119**, 183–194.

[38] L. Wang, A. Azizi, T. Xu, S. R. Kirk and S. Jenkins, *Chem. Phys. Lett.*, 2019, **730**, 206–212.

[39] L. Guillaumes, P. Salvador and S. Simon, *J. Phys. Chem. A*, 2014, **118**, 1142–1149.

[40] J. M. Guevara-Vela, E. Francisco, T. Rocha-Rinza and A. Martín Pendás, *Molecules*, 2020, **25**, 4028.

[41] S. J. Davie, P. I. Maxwell and P. L. A. Popelier, *Phys. Chem. Chem. Phys.*, 2017, **19**, 20941–20948.

[42] H. Fischer and H. Kollmar, *Theoret. Chim. Acta*, 1970, **16**, 163–174.

[43] A. A. Voityuk and N. Rösch, *J. Phys. Chem. A*, 2000, **104**, 4089–4094.

[44] J. J. P. Stewart, MOPAC2016, http://OpenMOPAC.net.

[45] M. Gaus, A. Goez and M. Elstner, *J. Chem. Theory Comput.*, 2012, **9**, 338–354.

[46] A. Tkatchenko and M. Scheffler, *Phys. Rev. Lett.*, 2009, **102**, 073005.

[47] B. Hourahine, B. Aradi, V. Blum, F. Bonafé, A. Buccheri, C. Camacho, C. Cevallos, M. Y. Deshaye, T. Dumitrică, A. Dominguez, S. Ehlert, M. Elstner, T. van der Heide, J. Hermann, S. Irle, J. J. Kranz, C. Köhler, T. Kowalczyk, T. Kubař, I. S. Lee, V. Lutsker, R. J. Maurer, S. K. Min, I. Mitchell, C. Negre, T. A. Niehaus, A. M. N. Niklasson, A. J. Page, A. Pecchia, G. Penazzi, M. P. Persson, J. Řezáč, C. G. Sánchez, M. Sternberg, M. Stöhr, F. Stuckenberg, A. Tkatchenko, V. W. z. Yu and T. Frauenheim, *J. Chem. Phys.*, 2020, **152**, 124101.

[48] F. Jimenez-Gravalos, J. L. Casals-Sainz, E. Francisco, T. Rocha-Rinza, A. Martín Pendas and J. M. Guevara-Vela, *Teor. Chem. Acc.*, 2020, **139**, 5.

[49] J. M. Guevara-Vela, R. Chávez-Calvillo, M. García-Revilla, J. Hernández-Trujillo, O. Christiansen, E. Francisco, A. Martín Pendás and T. Rocha-Rinza, *Chem. Eur. J.*, 2013, **19**, 14304–14315.

[50] V. M. Castor-Villegas, J. M. Guevara-Vela, W. E. Vallejo-Narvaez, A. Martín Pendas, T. Rocha-Rinza and A. Fernandez-Alarcon, *J. Comput. Chem.*, 2020, **41**, 2266.

[51] A. S. de la Vega, T. Rocha-Rinza and J. M. Guevara-Vela, *ChemPhysChem*, 2021, **22**, 1269–1285.

[52] T. Steiner, *Angew. Chem. Int. Ed.*, 2002, **41**, 48–76.